The Pennsylvania State University

The Graduate School

INCORPORATING NOVEL SPRUE DESIGN AND ADDITIVE MANUFACTURING TECHNIQUES TO IMPROVE NICKEL ALUMINUM BRONZE CASTINGS

A Thesis in

Mechanical Engineering

by

Nicholas A. Soares

Submitted in Partial Fulfillment
of the Requirements
for the Degree of

Master of Science

May 2022

The thesis of Nicholas A. Soares was reviewed and approved by the following:

Guha Manogharan
Assistant Professor of Mechanical Engineering
Thesis Advisor

Robert Voigt
Professor of Mechanical Engineering

Daniel Haworth
Professor of Mechanical Engineering
Head of the Department of Mechanical Engineering

ABSTRACT

Metal casting is one of the oldest forms of manufacturing, dating back thousands of years. While new techniques and alloys have been developed, the basic casting process has remained mainly unchanged since its inception. The four basic steps of casting are pouring, filling, feeding and cooling. Even today, metal casting can still result in defects and discarded castings. However, modern technologies have shown to have a place in metal casting, such as 3D printing sand molds and simulating castings before pouring. Such applications of these technologies can be with metals such as Nickel-Aluminum Bronze, which is used for critical marine and naval parts. This work will dive into the history and current state of the metal casting industry as well as how the process can be refined and advanced by leveraging modern technologies. It will focus on NAB as the main alloy studied, as its applications would directly benefit from further improved material properties. Flow simulations, CT analysis, mechanical testing, and SEM imagery were studied to determine the effects novel sprue geometries have on the sand casting process. The effects of straight, parabolic and helical sprue geometries on thin-walled castings were examined. It was found that helical sprue geometry resulted in the lowest percentage of casting defects while exhibiting an increase in flexural modulus in the casting over the straight sprue. A columnar grain microstructure was seen to be similar among all samples, likely due to a similar cooling rate during casting.

TABLE OF CONTENTS

LIST OF TABLES

LIST OF FIGURES

ACKNOWLEDGEMENTS

I would like to thank Dr. Guha Manogharan for helping to make this work possible through his support, guidance, and dedication. I would also like to thank Dr. Robert Voigt for offering his thoughtful comments and suggestions. A special thanks is also given to Phil King, as well as all members of the SHAPE Lab, in their help and motivation throughout my time at Penn State. Finally, I would like to thank all of my friends and family members who have supported me over the years in the pursuit of my academic achievements.

This material is based upon work supported by the Office of Naval Research under Award No. ONR 139977. Any opinions, findings, and conclusions or recommendations expressed in this publication are those of the author(s) and do not necessarily reflect the views of the Office of Naval Research.

INTRODUCTION

Metal casting is one of the world's oldest manufacturing methods, with origins tracing back thousands of years[8,9]. Prior to its existence, metal objects were difficult to craft and prohibitively expensive, especially in large quantities. Throughout the centuries, metal casting has been both a driver and enabler of technological advancement. Casting helped to quickly grow cities taller, made durable goods more available and affordable, and allowed for rapid long-distance travel. Modern manufacturing techniques not only rely on metal casting to mass-produce goods, but casting is also necessary for the creation of machinery and tooling. It was estimated that in 2018, the metal casting industry held a $123.8 billion market share worldwide and was projected to continuing growing at over 5% annually through 2025[10]. As the global population continues to rapidly increase, casting is vital to not only ensuring everyday goods are available, but also necessities such as food and water. However, as technology rapidly advances, and goods become more individualized, traditional casting methods are becoming quickly outdated.

The long leads times commonly found in these traditional methods can range from weeks to months, much of which is dedicated to pattern or tooling creation. These lengthy turnaround times are creating a bottleneck in the design and production of modern goods. Within the last few decades, rapid production methods such as additive manufacturing (AM) and 3D-printing (3DP) have become commonplace in the design process for their rapid prototyping (RP) capabilities. These methods are able to significantly decrease lead time from months to days. Researchers have been investigating the potential for incorporating these technologies into the metal casting industry to increase both the efficiency of casting production as well as capabilities of what can be produced. Such technologies include 3D sand-printing (3DSP), wax pattern creation through fused-deposition modeling (FDM), and ceramic shell creation using power bed fusion (PBF).

As sand casting is one of the most popular casting methods, 3DSP has been the focus of a number of recent studies to determine its utility in the casting process. Given the geometric advantages of 3DSP, novel sprue geometries were investigated for their potential to decrease defect formation such as entrained air and oxide film inclusions[11]. Additionally, the potential for controlling local cooling rates within the casting leveraging this geometric freedom has been explored[12,13]. Traditionally, silica sand has been used in foundries for the creation of sand molds. However, recent health and environmental regulations have caused a shift to non-silica sand. Thus, non-silica-based sand has been applied to the 3DSP process[11,14], as well as the use of reclaimed foundry sand[15]. Also, the effect of 3DSP on the part surface finish has been compared to the use of traditional methods for sand mold creation. Given the significant reduction in lead time using 3D sand-printing, the process has potential to make sand casting more accessible to individual or low quantity production runs. This has a number of notable uses, such as rapid prototyping with metal components, out-of-production parts for maintenance of old systems, and emergency repair in isolated locations. Another significant advantage to 3DSP is the ability to work with a wide range of metals, just as in traditional sand casting.

One of these novel alloys is Nickel Aluminum Bronze (NAB), copper-aluminum alloy, which is often used for Naval and marine applications due to its good corrosion resistance[16–18]. Such applications of NAB include bushings, bearings, propellor hubs, and piping[19]. Research has shown the complex microstructure of NAB is closely tied with its corrosion resistance[20]. Thus, much work has been done to investigate methods that can even further control its microstructure post-casting. A few of these methods include controlled cooling rates, heat treatment, and friction surfacing. One of the main contributors thought to negatively impact corrosion resistance is the β' phase (or retained β). β' is a dense, martensitic phase that is the result of rapid cooling or quenching. As the cooling rate is increased, the high temperature β phases is only partially transformed into the copper-rich α phase or intermetallic κ_{III} precipitate. Hot working techniques, such as annealing, have shown promise in reducing this hard β' phase and annealed samples exhibited better corrosion resistance[20,21]. Additionally, friction surfacing with NAB has been demonstrated to decrease cavitation erosion and reduce wear[22]. NAB castings are also susceptible to traditional casting defects, along with these alloy-specific challenges.

Defects in metal casting has been a long-studied subject, as the accurate prediction of mechanical properties of a cast part is often crucial. Defects in casting can result from a number sources but can be broadly categorized into the four main stages of casting: pouring, filling, feeding, and solidification. During pouring, an oxide film layer is created on the surface of the molten metal that is in contact with the air. As the metal is poured into the casting cavity, this film is mixed into pool of metal due to turbulence and becomes trapped inside the casting, creating oxide film inclusions. This turbulence can also cause incomplete fusion of metal that has begun to cool, which results in local area of reduce mechanical properties. As the cavity is filled, run-out can occur due to gaps or cracks in the mold. If the pouring temperature is not high enough, premature cooling may block portions of the cavity from filling entirely, called misruns. As the part fills and begins to cool, large interior volumes can remain at high temperatures after the exterior has sufficiently cooling, called hot spots. This results in part shrinkage and porosity. As technology continues to advance, various methods such as numerical optimization have been leveraged to reduce defects in each stage of the casting process.

The introduction of additive manufacturing techniques into the metal casting process provides the potential for significant improvements in each state of the casting process and reducing defect rates. A major benefit to these AM processes is the ability to rapidly redesign a mold geometry digitally, rather than fabricating physical components. It then possible to accurately simulate the casting with computational software as opposed to the common trial-and-error approach on the foundry floor. Given these advantages, much work is being done to leverage the benefits of AM. Novel sprue geometries have been shown to reduce in-gate velocity, thus reducing as part defects due to turbulance[11]. Computer simulations have been used to improve runner and gating networks, and in some cases decreasing rejection rates by over 30%[23,24]. Researchers have used evolutionary topology optimization to redesign the size and location of risers to reduce defect rates while improving casting yield[25,26]. The creation of lattice

networks for mold design has allowed for adjusting local cooling to counteract hot spots while reducing the required material[12,13,27].

Still, many foundries have not been fully able to take advantage of these new technologies for several reason.. The first being the infrastructure cost, as current machinery and supply chain logistics are difficult to restructure overnight. The second reason lies in the cost of part rejection, with scrap parts easily being remelted for future use with minimal financial setback. However, as the world advances the greatest cost will be in the time spent on inefficient practices. The goal of this thesis is thus to shed light on the potential benefits and sense of urgency that these new technologies possess for the science of metal casting. This work aims to identify and investigate a specific application of some of these methods, being sand casting Nickle Aluminum Bronze alloy using additive techniques to compare unconventional sprue geometries with 3DSP. Additionally, the role many of these technologies has in improving each stage of the casting process will also be covered.

CHAPTER 1

The Science of Metal Casting in the 21st Century

Abstract

This review details the advancements in the science of metal casting and explores the potential for further innovation through leveraging new technologies, such as additive manufacturing (AM) and rapid prototyping (RP). While metal casting originated thousands of years ago, modern casting techniques consist of the same four basic stages: pouring, filling, feeding, and solidification. Since the various methods for casting employ either a permanent or expendable mold, this provides two groups for broad classification. Larger foundries often leverage select new technologies and software to reduce costs and production times; however, metal casting can still be a labor-intensive process. The upfront cost and process changes requires for these technologies has made it difficult for some foundries to fully adopt these processes. This paper explores these technologies and discusses how they might impact the science of metal casting and push it fully into the 21st century, with a specific focus on the four main stages of casting and investigates their potential to revolutionize fields outside of casting.

Introduction

The science of metal casting dates back to nearly 5000 BC, with the first known castings being small decorative pieces made from bronze[8,9]. The technology eventually expanded to aid in making simple tools and weapons out of iron and steel[8,9]. Today, metal casting has become a staple of modern manufacturing, producing everything from children's toys to engine blocks. The American Foundry Society (AFS) reported that 10.7 million tons of castings were produced in 2017 in the U.S. alone[28]. Metal casting is often used for large-scale manufacturing as it can economically produce near net-shape parts on a large scale. The AFS states that roughly 90 percent of durable goods produced today contain cast metal components[29]. As a result of this large market share, metal casting was estimated to be a $123.8 billion industry globally in 2018, and was projected to grow over 5% annually through 2025[10]. The various techniques used for casting can be broadly classified into two major categories: expendable mold casting and permanent mold casting. As the names imply, expendable mold casting employs single-use molds, often made of sand or clay, which are broken to release the final part. In contrast, permanent mold casting processes use reusable molds, usually made of a metal alloy with a high melting point. Depending on the metal alloy and process temperatures, the lifecycle of permanent molds ranges from 10,000 to 120,000 uses[30].

Research Gap

Current research has focused on improving each stage of the casting process to increase yield and reduce defects (Figure 1.1)[11,15,31–33]. Most foundries have leveraged computational fluid dynamics and solidification software (i.e. Flow-3D Cast) to optimize risers to reduce material waste[26,34]; however, there are still many opportunities for foundries to lower long-term costs while increasing casting capabilities. With current lead times ranging from weeks to months, traditional metal casting is not advantageous for consumers requiring custom parts in small batches. This is a bottleneck in most design processes that require metal components. Many of the proposed techniques leverage AM and include 3D printing sand molds for sand casting[11,31–33,35] and wax patterns for investment casting[25,36–38]. This paper aims to shed light on these technologies that have the potential to cast more complex geometries in significantly less time, benefiting both the foundries and consumers. The goal of this paper is to investigate the current state of metal casting science and identify major areas of improvement in each of the four basic stages of the process. This paper will explore the role modern technologies, such as additive manufacturing, can have in advancing the efficiency, quality, and capabilities of casting science.

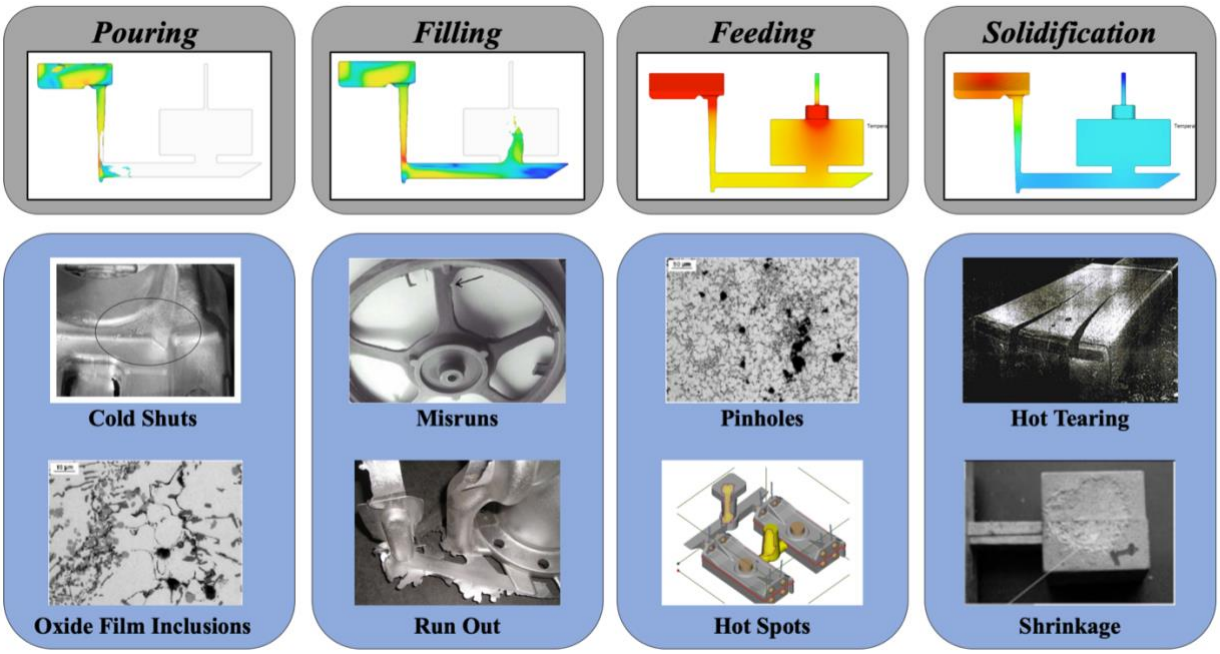

Figure 1.1. Common casting defects occurring in each stage of the casting process, such as Cold Shuts[1], Oxide Film Inclusions[2], Misruns[3], Run Out[4], Pinholes[2], Hot Spots[5], Hot Tearing[3], and Shrinkage[6]

Expendable Mold Casting Methods

The earliest known forms of casting used expendable molds, often made from a sand and clay mixture, to produce metal castings[8]. Many of these early castings were made using a technique called investment casting (IC), also known as lost wax or precision casting. The first step in this process is to create a ceramic mold around a wax pattern. The wax is then melted out by heating the mold and molten metal is poured into the empty shell. Once cooled, the shell is broken to retrieve the casting. Investment casting has been shown to have the excellent dimensional accuracy and surface finish when compared to other casting methods[39]. This method allows complex parts to be cast with wall thicknesses as thin as 0.5 mm[38]. However, the final casting is very sensitive to the quality of the wax pattern; any defects in the wax pattern will transfer to the metal casting. While the lost wax method is able to produce very detailed parts, this technique tends to be more expensive than other casting methods, with tooling costing as much as US$40,000[38]. IC can also be a long process, requiring a 40 to 50-week lead time in some cases[38], as both wax patterns and ceramic molds need to be made. Environmental regulations have also sparked change in certain aspects of this process, namely in the wax and ceramic mold mixtures due to use of toxic materials[40].

Sand casting (or sand molded casting) is another early form of metal casting in which a single-use sand mold is created in multiple parts, usually a top and bottom half, called the cope and the drag, respectively. This mold is formed by densely packing sand around the pattern and then removing it to leave a cavity. A major benefit to sand casting is the ability to cast most metal alloys in a wide range of sizes. As such, sand casting is often chosen when casting large items such as engine blocks. Another benefit is the pattern in sand casting can be reused (called a permanent pattern), as opposed to investment casting where a new pattern is required for each casting[9]. A permanent pattern uniquely allows metal components to be easily copied as the original part can be used as the pattern. This method is also relatively inexpensive compared to other metal casting methods, accounting for nearly 70% of total casting today[14]. However, the dimensional accuracy and surface finish quality of this technique are not as high as other forms of casting[39]. There have been many notable advancements in sand casting to increase the speed and efficiency of this process. “Green sand” is one of these innovations in which the sand is initially wet (giving it its “green” name) and instantly dries when it comes in contact with the molten metal[41]. This allows molds to be made more efficiently but it is only economically feasible for large-scale production runs. For individual castings or small batches, the possibility of 3D printing sand molds has been explored, dramatically reducing the lead time for a casting from months to weeks[11,31,42]. This method of producing molds and tooling additively allows for a drastic reduction in upfront lead times, but requires additional time for each casting, making it less suitable for high-volume production.

Permanent Mold Casting Methods

Die-casting is the most common form of permanent mold metal casting. Most die casting is done by forcing liquid metal into the mold cavity at a high pressure, although low pressure die casting is also used[42]. The metal used for the mold must have a higher melting point than the metal being cast to avoid melting the mold during casting. This form of casting is mostly reserved for high production quantities, as the tooling and molds required are often very expensive, with cost estimates from the Lakeshore Die Cast company ranging from $15,000 to $150,000[43]. For large quantities, this method is often economical while also producing parts with an excellent surface finish. Another notable advantage to this method is the ability to cast thin walls up to 0.2 mm[44]. However, the limitations of die casting are mainly found in the die itself, as the metal alloys that can be used for casting are limited by the melting point of the die. As a result, non-ferrous metals are often used. Ferrous metals can also be used; however, they are not as common due to their high pouring temperatures, which damage the die and reduce its lifespan. While larger parts such as engine blocks can theoretically be die-cast, many applications of die casting are smaller components, as the method is only economically viable when parts are about 75 pounds or less[45].

Main Stages of Casting

The entire casting process can be separated into two major stages, the design stage and casting stage, as shown in Figure 1.2. The design stage involves first designing the part and mold, often using computer-aided design (CAD) software. Computer simulations are then run to ensure the casting will fill properly without defects before the mold is made. Once the mold is created, the next stage in the process is casting, which contains the four main steps: pouring, filling, feeding, and solidification[31]. While there are many different approaches to creating the mold, the casting stage is often very similar. Over the last few decades there have been significant technological advancements in each step of the casting process. Such advancements include 3D-printed sand molds, non-conventional sprue design, optimization of riser and runner networks, and hot-tearing analysis during cooling. A selection of these advancements will be discussed in detail in later sections.

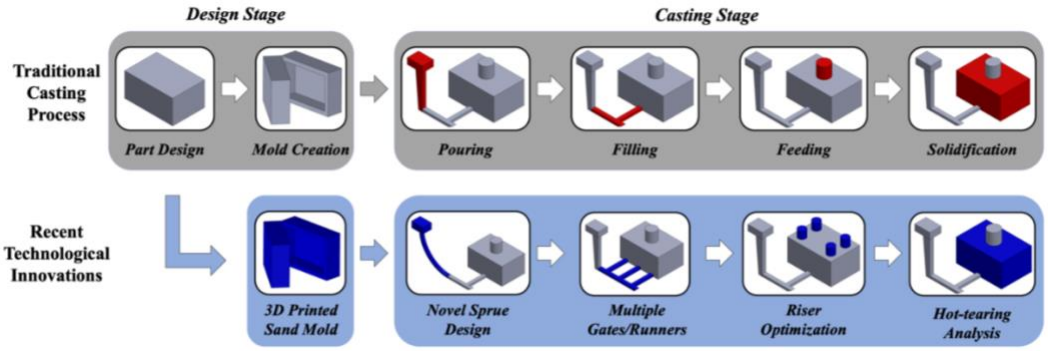

Figure 1.2. Overview of the traditional casting process with select recent technological developments for each major stage

Once the mold is made, the first step in the casting stage is to pour liquid metal into the mold. This is often done by a channel, called a sprue, that directs the molten metal from the pouring basin to the network of runners at the base of the mold, as shown in Figure 1.3. Most castings have simple geometries for the sprue which can lead to defects (i.e. cold shots, oxide film inclusion, etc.)[11]. As this is a major issue in casting, recent research has focused on redesigning sprues using complex parabolic and conical-helix geometries, reducing defects by up to 99% in some alloys[11]. In sand casting, this process is often gravity-fed, meaning the molten metal is not pressurized during pouring. This is done to avoid unnecessary force on the sand mold, which is more delicate than metal tooling. In contrast, most die-casting and some investment casting processes utilize pressurized pouring, in which the liquid metal is forced into the mold. This is advantageous as it deceases the pour time and reduces the chance for premature cooling, which can lead to misruns[46].

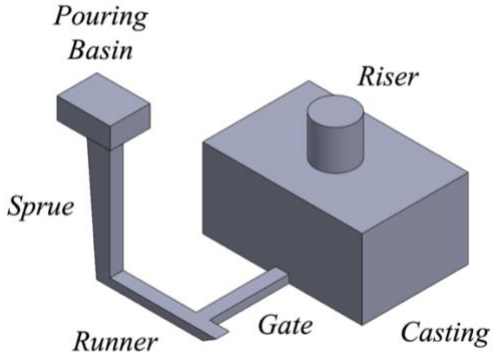

Figure 1.3. Basic metal casting diagram, showing the pouring basin, sprue, runner, gate, and riser components, along with the casting itself.

After the molten metal has entered the mold system, it must be directed throughout the cavity to fill the entire shape. This is done through the use of a channel called a runner. Runners often run parallel to the cavity with one or more gates, which are smaller channels that connect the runner to the mold cavity (Figure 1.3). While these gates can be connected to the top, side or bottom of the mold, gating is important to reduce casting defects[46]. This system aims to evenly distribute metal to all parts of the mold; however, premature cooling can prevent the metal from completely filling the cavity, which is called a misrun. In most cases, misruns are due to poor runner and gating design, and result in scrapping the entire casting. Researchers have investigated this process to reduce misruns, and have suggested more optimal designs such as including multiple gates and runners[23,47].

As the mold cavity is filled, the metal casting begins to cool. The casting will shrink as a result of this cooling, losing its dimensional accuracy and potentially creating porosity. To combat these issues, reservoirs called risers are used to continuously re-fill the mold cavity as the metal shrinks. Risers are additional cavities in the mold that fill with molten metal and can either be connected to the runner network or the mold cavity itself (Figure 1.3). The riser is often categorized as “open” if it is exposed to the atmosphere, otherwise, an entirely internal riser is

called “blind”[46]. The main challenge in effective riser design is that the metal in the riser cannot cool before the casting has cooled. If the riser does cool first, then the casting and riser have effectively reversed roles, with the casting feeding the riser instead of vice-versa. While a very large riser may fulfill this requirement, the amount of metal required for each casting should be minimized to reduce costs. Software simulations help calculate the minimum required riser volume, but riser location is another complex design consideration. Various methods have been investigated to optimize feeding systems and riser design to reduce both the material waste and likelihood of defect formation[23,48]. The final step in the casting process is the solidification and cooling of the casting. Thicker sections of the casting may cool at different rates than thinner sections, which can result in uneven cooling and shrinkage. Uneven cooling can not only result in risers not functioning properly, but also produce hot tears in the final part. Hot tears are small separations in the casting that often result from restriction during shrinking or in feeding. This complex issue has been explored by numerous researchers[49,50]; however, it is still one of the most common defects in casting.

Additive Manufacturing

Additive manufacturing (AM) began in the 1980s with rapid prototyping in mind, combining computer software with earlier electronic technology developed in the 1970s[14,51]. As the AM industry developed, the applications for AM extended to rapid tooling (RT) and rapid manufacturing (RM)[14,32]. Within the last few decades, AM techniques have been applied to the manufacturing of metal components. There are two distinct methods for this application, direct metal AM and indirect metal AM[52]. Direct metal AM is the fabrication of metal parts using additive techniques (i.e. directed energy deposition (DED) and powder bed fusion (PDF))[53]. Whereas indirect metal AM involves replacing traditional tooling methods used in metal processing with additive techniques[14]. AM in metal casting falls into this category. There are three main methods that AM is used in metal casting. The first is leveraging material extrusion AM to print wax patterns for investment casting[25]. The next method is printing reusable plastic patterns for sand casting[54]. The final method is printing the mold itself which can be done for both sand casting and die casting[31,55–57].

Wang et al.[25] studied the feasibility of AM wax patterns for the investment casting of a complex impeller casting. This study compared two materials, photosensitive resin and high-impact polystyrene (HIPS) with select laser sintering (SLS). It was determined that photosensitive resin was not suitable for complex casting due to shell cracking, but the HIPS proved to be a viable option for printing wax patterns[25]. The authors concluded that using AM wax patterns for investment casting is feasible and has the potential to shorten lead time, lower costs, and make metal casting a viable option for small production quantities[25]. Topology optimization of 3D printed wax patterns was investigated by Wang et al.[38] to create parts with reduced weight and increased mechanical performance. The authors were able to achieve this by redesigning a bracket to reduce its weight by 68% while increasing its safety factor by 20%[38]. In addition to this, the required lead time was decreased by over 90%[38].

The other method of AM for metal casting that involves printing patterns is FDM printing of sand casting patterns. Unlike for investment casting, however, the patterns printed for sand casting are reusable. Henderson et al. investigated the advantages of using FDM printed patterns compared to traditional machined patterns[54]. The FDM patterns resulted in a reduction in both cost and lead time, as well as required no labor once the print was setup. One issue that the printed pattern had was with extraction from the sand. When the researchers first tried to remove the pattern from the mold sand remained attached to the mold. However, this was solved by reducing the surface roughness of the pattern with manual tools[54]. Overall, the cost was reduced by 7% and the lead time was reduced by 21%, while the part geometry was more complex than if produced via traditional methods[54].

The final area where AM and metal casting intertwine is with additively manufacturing molds. For die casting this is accomplished through using direct metal AM to print a reusable die, while for sand casting a single use sand mold is printed using binder jetting (a process known as 3D Sand Printing)[31,55–57]. There have not been very many studies investigating direct metal printing for die casting. One study focused on using direct metal printing to better control cooling for die casting. Direct metal printing facilitates this by allowing cooling channels to be printed into the die[57]. What the researchers of this study acknowledged has not been examined and is important to study, however, is the lifespan of printed dies compared to traditional dies. The researchers stated that their die performed well for 2000 casting runs but that they did not know how it would fair for hundreds of thousands more runs[57]. On the other hand, 3D Sand Printing (3DSP) has been the most researched area of AM in casting. 3DSP is a binder jet process where sand and binder are deposited layer by layer to additively construct the mold and has been leveraged to improve numerous areas of sand casting[31,51]. The four main areas it has been used for are: producing small batches of molds, making complex geometries, improving cooling, and manufacturing cores[12,31,32,55].

For small batches of molds, the most significant advantage that 3DSP offers compared to traditional casting is that it does not require permanent tooling. As a result, the cost per mold is greatly reduced, as well as the lead time for the molds. However, for large batches of molds 3DSP loses both of these advantages because the tooling cost per mold decreases and the molds can be made using traditional methods, which greatly decreases the lead time. For instance, an ExOne S-Max Pro can take up to 12 hours to print a mold, depending on its size[58], while a Disa Disamatic C3-350 can produce up to 350 molds per hour[59].

The next advantage of 3DSP is its ability to make complex mold geometries. Sama et al. investigated the potential for non-conventional sprue geometries to reduce the metal velocity and turbulence during pouring and filling. Various novel sprue geometries were simulated, such as parabolic and conical helix, to determine the most advantageous design. It was found through simulation, and validated through experimental tests, that a conical-helix sprue design was able to best control turbulence and keep flow velocity below the critical value of 0.5 m/s, reducing the volume of defects for stainless steel castings by 99.5%[11]. 3DSP can also be used to make intricate geometries that reduce the weight of the castings. Wang et al. investigated this by using

topology optimization in conjunction with 3DSP resulting in a weight reduction of a bracket by 50%[14].

Another area where 3DSP outperforms traditional casting is in mold cooling and solidification. Traditionally, metal casting has been plagued with issues in cooling and solidification, leading to high amounts of failed castings. Recently, however, researchers have investigated leveraging 3DSP to make ribbed castings that facilitate even cooling. Kang et al. investigated this by comparing the cooling of a traditional casting to a ribbed casting. They found that the ribbed mold decreased the cooling time while also reducing the quantity of defects, residual stresses, and deformation[12].

The final area where 3DSP has changed the metal casting industry is with core production. 3DSP has facilitated core consolidation allowing for multiple cores to be combined into one core which has reduced the complexity of assembling molds and cores. In fact, due to the small size of many cores, and the benefits of core consolidation, 3DSP can be more efficient and cost effective at the large scale production of cores[55].

Casting Simulation and Optimization

Traditionally, most molds are created through a trial and error process at the foundry to ensure there are no defects in the final product[60]. This is a time-consuming, and expensive, process that has many variables such as pouring temperature, runner/gating network, and casting alloy. It is also difficult to record the dynamics of the metal flow during casting and any defects on the interior of the part. As large-scale computing becomes more accessible, computer simulation software has been leveraged to make this process more efficient. Each step in the casting stage has been studied using simulations to investigate potential signs of defect formation and optimize the mold geometry. Popular casting similar software includes MAGMASOFT, ProCAST, and FLOW-3D Cast. The most common numerical methods employed by these and other programs are finite element method (FEM) and finite-difference method (FDM)[24].

The filling and feeding system is a crucial component of the casting mold, as it is estimated 90% of defects are caused by improper design of these features[23]. Runner and gating network optimization of a high-speed rotor was investigated through computer simulation and numerical methods by Huang et al.[24]. The authors were able to simulate the effects of various parameter changes, such as pouring time and mold temperature, on the casting quality. The best design was then experimentally validated to show the predicted decrease in defect formation and casting yield increase[24]. Nimbulkar et al.[23] used simulation techniques to optimize the gating feeding systems to reduce the rejection rate of sand casting. The authors found that through redesigning the risers and gating network through simulations they were able to reduce the rejection rate by 30% while increasing the yield percentage[23]. Other researchers, such as Wang et al.[25] and Tavakoli et al.[26] used simulation software and methods such as evolutionary topology optimization to redesign the riser location and sizing to increase casting yield by over 50% and minimize defects.

CHAPTER 2

Incorporating Novel Sprue Geometries in 3D Sand-Printed Molds for Nickel Aluminum Bronze Castings

Abstract

Nickel-Aluminum Bronze (NAB) is a commonly cast metal for marine and other naval applications due to its high strength and corrosion resistance. While traditional casting methods have been refined over time, the basic process has remained mostly unchanged. Specifically, this process includes the use of simple straight sprues. Recent studies have shown that incorporating novel sprue geometries can reduce defects such as entrained air and oxide film inclusions. These novel sprue geometries include parabolic and helical configurations. This study investigates the potential in leveraging 3D-printing technology for sand casting to improve the microstructure and material properties of NAB. Initial casting simulations will be used to during the selection stage, and CT scanning, SEM imagery, and 3-point bending tests will be used for data collection.

Background and Motivation

Nickel-Aluminum Bronze (NAB) is a copper-aluminum alloy with a nominal composition (wt%) of 5% iron, 5% nickel, 10% aluminum, and remainder copper[17,20]. NAB is well-suited for marine and naval applications due its corrosion and biofouling resistance, along with moderate strength and good material properties[16–18]. Additional factors such as a low coefficient of friction, resistance to oxidation at high temperatures and low magnetic permeability have also proven to be advantageous[17]. Common marine and aerospace applications for NAB include bushings, bearings, propellor hubs, wear rings, and piping[19]. As-cast NAB has a complex microstructure, usually consisting of α and β' (retained β) phases, along with various intermetallic κ precipatates[20,61]. The resulting microstructure has been shown to be heavily dependent on the casting method and cooling rate, along with the aluminum content of the alloy. Specifically, the β' phase has been known to lead to increased corrosion[20].

The microstructural evolution for room-temperature (equilibrium) cooling is known[20,62], as seen in Figure 1.1[7]. During casting, the high-temperature β phase is initially found throughout the alloy at temperatures exceeding 1030ºC. As the temperature falls below this threshold, the α phase is formed within the β phase. The α phase is a copper-rich solid with FCC structure. As the casting cools below 930 ºC, the κ_I or κ_{II} (depending if Fe content is greater or less than 5 wt%, respectively) precipitate begins to form in the β phase. Both intermetallic κ_I and κ_{II} phases are globular, with the κ_{II} phase being notability finer. The fine, Fe-rich κ_{IV} precipitate partially forms in the α phase below 860 ºC. Once the casting cools to below 800 ºC, the β phase completely converted to the α and κ_{III} eutectoid, which is a NiAl-based phase with lamellar morphology. Thus, the microstructural makeup of the room temperature alloy contains only α and various κ phases. Increasing in the cooling rate results in only partial transformation of the β phase to κ_{III}, resulting in retained β, also known as β'.

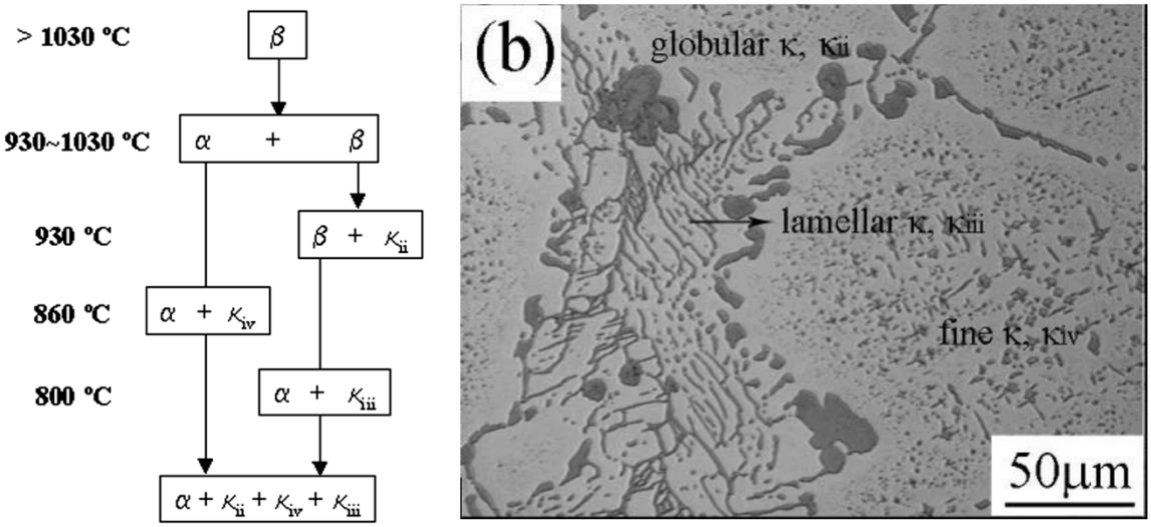

Figure 2.1. Typical microstructural phase transformations for NAB undergoing room-temperature cooling (a) and resulting final microstructure (b). Source: Oh-Ishi et al.[7]

Much work has been done to investigate controlling the microstructure of NAB, as microstructural makeup has been shown to have a significant impact on its corrosion resistance[16,20,21,61–64]. Previous studies involved various heat treatment and annealing techniques, adjusted cooling rates, change in chemical composition, friction surfacing, and friction stirring. Wu et al. varied heat treatment levels on NAB vacuum melted samples to investigate the erosion-corrosion resistance. Different cooling methods were used, including room temperature, furnace cooling and quenching. They found that the erosion-corrosion resistance increased with the inclusion of hard phases, such as β'. Anantapong et al.[20] annealed NAB samples at 675 ºC and heat treated them to various temperature between 750 ºC and 1000ºC, with rapid cooling. The authors found that no β' phases were present after annealing and microstructure was heavily influenced by heating temperature. Both high heat treatment temperatures and cooling rates resulted in larger amounts of β' phase. Ai et al.[21] characterized the microstructure of hot extruded rods of NAB that were heat treated through different processes, including quenching, normalizing, aging and annealing. While annealing was shown to reduce tensile strength and hardness, it eliminated the β' phase through transforming it into α and κ phases. The annealed samples had the greatest resistance to corrosion, due to the elimination of the β' phase.

Friction surfacing[22] and friction stirring[65,66] have also been shown to improve the mechanical properties. Hanke et al. used friction surfacing to apply an NAB coating on a metallic stud to investigate the rate of cavitation erosion. The single-layer coating was shown to have increased resistance to cavitation erosion and reduction in wear rate. Ni et al.[65,66] used friction stir processing to refine the microstructure of cast NAB and found it to have increased static corrosion resistance along with reduced porosity.

The aim of this work was to investigate the properties of NAB alloys cast using 3D sand-printed molds with novel sprue geometries. These complex sprue geometries have been shown for other metal alloys to reduce entrained air and oxide film inclusions as well as increase the

mechanical strength of the cast part. The general overview and scope of this work is shown in Figure 2.2. Step 1 involves the creation of the CAD models. Step 2 will focus on casting simulations and narrowing of scope. Step 3 will be the castings of the NAB plates. Step 4 will use computed tomography (CT) scanning determine the number of defects in the castings. Step 5 will employ scanning electron microscopy (SEM) to evaluate the microstructure of the castings as well as 3-point bending tests.

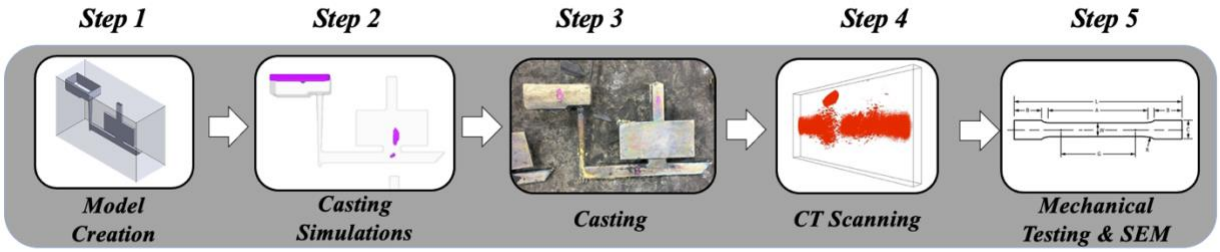

Figure 2.2. Overview of work, including model creation, casting simulations, casting, CT scanning, and mechanical testing & SEM imagery.

Methods

For this work, sand molds with various sprue geometries were 3D-printed to cast NAB plates which were analyzed using CT scanning, SEM imagery, and 3-point bending testing. The sprue geometries were chosen to be straight, parabolic and helical, based on work by Santosh et al.[31] and King et. al[67]. The helical and parabolic sprues were shown to reduce defects and oxide film entrainments when compared to the straight sprues. All models were created in SolidWorks and used the same plate castings with a height of 100mm, a width of 200mm (Figure 2.3), and then thicknesses of 10mm, 12.5mm, and 15mm, resulting in 3 simulations for each sprue geometry.

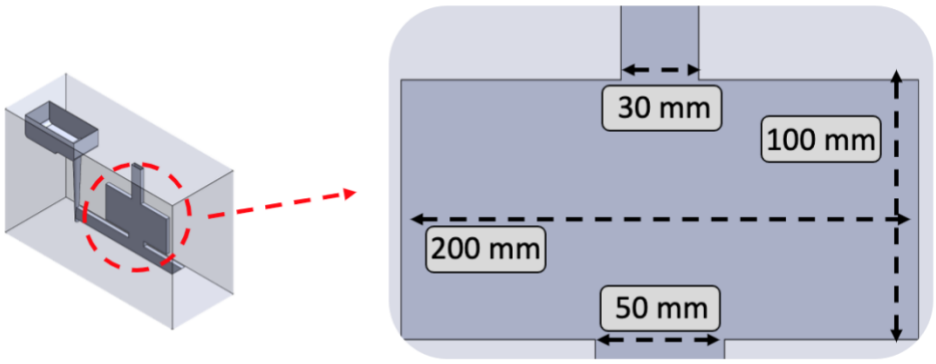

Figure 2.3. Plate dimensions for all simulations and castings of each thickness.

Each of the three sprue types: straight, helical, and parabolic (Figure 2.4) were combined with the three plate thicknesses for a total of 15 models. These simulations achieved two goals. First, they verified that initial hypothesis that the 3D sprue geometries would reduce in-gate velocity was correct. Next, they also determined the plate thickness to be used for casting. In the past, Sama et al.[11] used 10mm thick plates. However, because for this research additional mechanical and corrosion testing was going to be performed (tensile and corrosion testing), thicker plates were desired.

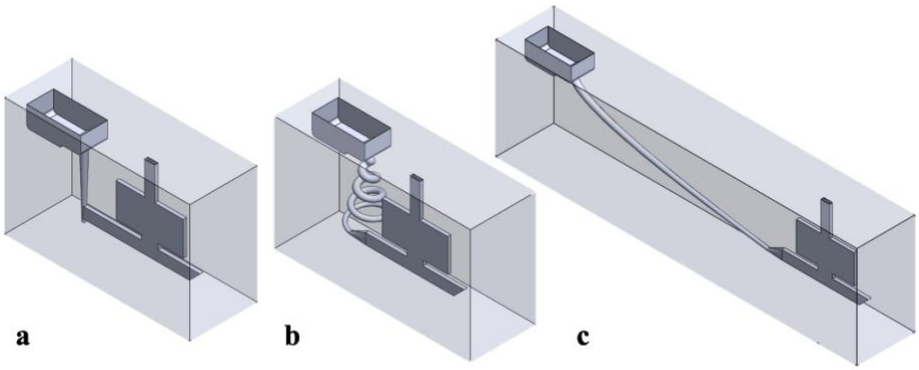

Figure 2.4. CAD models for 15mm plate castings with straight (a), helical (b) and parabolic (c) sprue geometries.

The straight sprue had slightly tapering diameter normal for a casting of this size. The parabolic sprue followed the relationship y = 0.2253x^(½) from x=0 to x=0.6744, shown in Figure 2.5. The total length of this parabola curve is 714.79 mm. This was determined using the Bernoulli equation (Eqn. 1) and solving for head loss in the energy equation (Eqn. 2).

$$P_{in} + \frac{\rho V_{in}^2}{2} + \rho g z_{in} = P_{out} + \frac{\rho V_{out}^2}{2} + \rho g z_{out} \quad \text{(Eqn. 1)}$$

$$h_l = \frac{V}{2g}\left(\frac{fs}{d}\right) \quad \text{(Eqn. 2)}$$

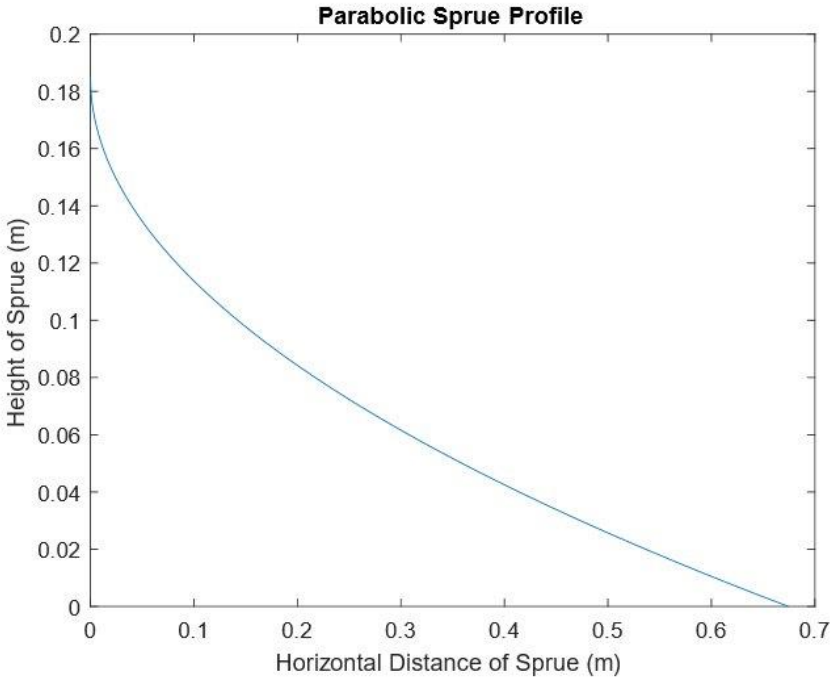

Figure 2.5. Height of sprue as a function of horizontal distance for the parabolic sprue.

The helical sprue is defined by the relationships: x = rt*cost(t); y = rt*sin(t); and z = z_0+mrt, with radius *r*, initial t_i and final step t_f, slope *m*, and the height z_0. The values for all variables are given in Table 2.1 and the 2D and 3D curves are shown in Figure 2.6.

Table 2.1. Parameters for helical sprue geometry, including radius *r*, initial step t_i and final step t_f, slope *m*, and height z_0

Variable	Value
r	1.99×10^{3}
t_i	0
t_f	25.77
m	3.59
z_0	185×10^{-3}

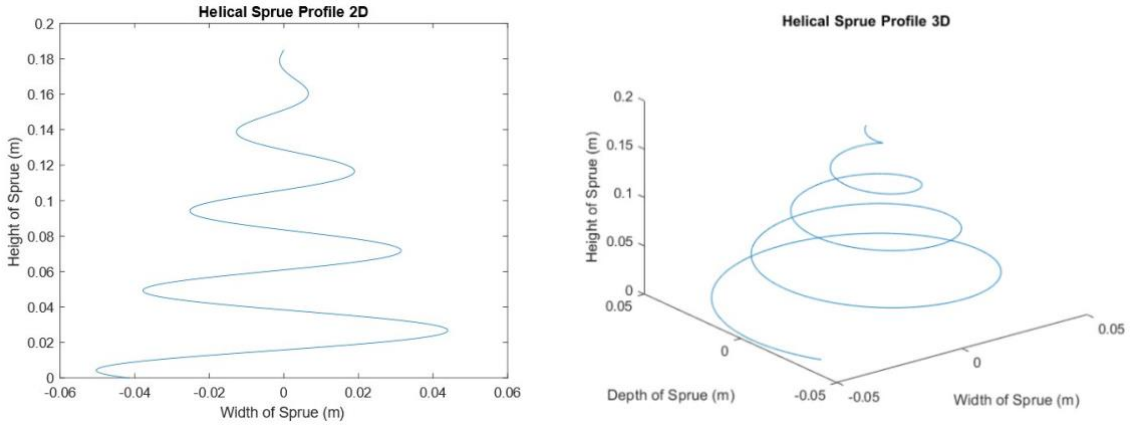

Figure 2.6. Height of sprue as a function of horizontal distance for the helical sprue with 2D (left) and 3D (right) projections.

Flow simulations of each model were completed in Flow3D-Cast to determine the average entrance velocity using a point probe. Based on Campbell et al.[46]'s work, the ideal in-gate velocity should be less than 0.5 m/s to sufficiently reduce defects and oxide film entrainments. The pouring conditions for the simulations are shown in Table 2.2.

Table 2.2. Pouring conditions for FLOW3D-Cast simulation for each sprue type.

	Straight	**Parabolic**	**Helical**
Pour Temperature (Celsius)	1160º	1247º	1160º
Flow Rate (m^3/s)	0.0005	0.0005	0.0005
Mesh Size (mm)	1.5	1.5	1.5

The final cast plates were determined to be 15mm x 100mm x 200mm in size for this study. Again, because of the additional tests that were conducted, as thick a plate as possible was desired. Five samples of each of the three sprue geometries were cast, for a total of fifteen castings. The castings were poured at Ashland Foundry using NAB alloy with chemical makeup: Cu 80.9 wt.%, Fe 4.03 wt.%, Ni 4.60 wt.%, Al 9.2 wt.%, Mn 1.0 wt.%, Si 0.03 wt.%, Pb 0.02 wt.%. All the plates were then imaged using computed tomography (CT) with a voxel size of 124 micron. A custom Python script leveraging OpenCV[68] in conjunction with Avizo[69] version 2020.2 was used to analyze the CT data. When the CT data was analyzed, each sprue design had one outlier, so those plates were removed from further analysis. Next, the plates were sectioned for SEM and mechanical testing using the configurations shown in Figure 2.7. Each sprue condition had one plate sectioned in each configuration for a total of 12 bending samples, tensile samples, and SEM samples.

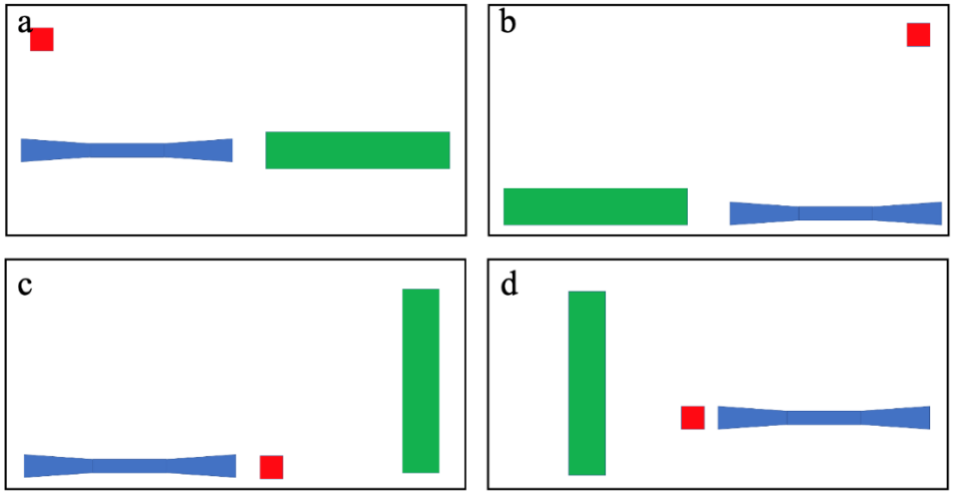

Figure 2.7. Configuration 1 (a), Configuration 2 (b), Configuration 3 (c) and Configuration 4 (d) showing the approximate locations and orientations for the tensile (blue), bending (green) and SEM (red) sections.

The tensile samples were ASTM E8 subsize coupons and the dimensions are given in Figure 2.8. This subsize was chosen as the plate thickness was too small for the full-size E8 sample. The bending samples were ASTM E290-14 and the dimensions are provided in Figure 2.9. The SEM sections were 10mm x 10mm and then polished to a surface roughness less than one micron (Figure 2.10).

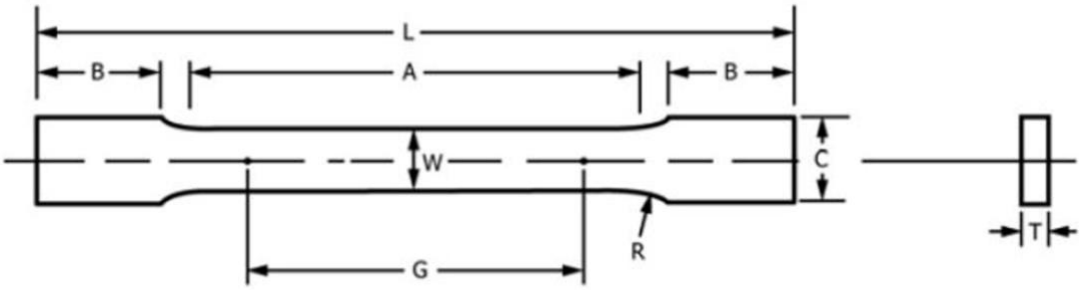

Dimension	L	A	B	W	G	R	C	T
Value (mm)	101	32	30	6	25	6.06	10	5

Figure 2.8. ASTM E8 subsize tensile coupon dimensions.

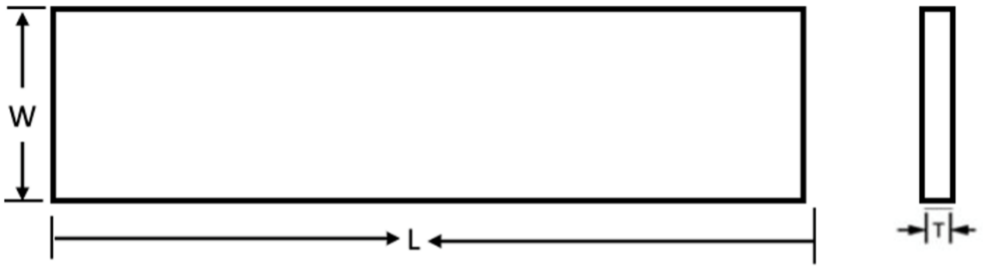

Dimension	L	W	T
Value (mm)	101	32	30

Figure 2.9. ASTM E290-14 bending coupon dimensions, including length (L), width (W) and thickness (T).

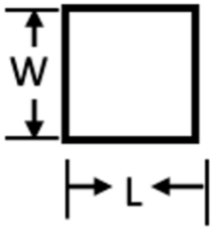

Dimension	L	W	T
Value (mm)	10	10	15 (as cast)

Figure 2.10. SEM test sample dimensions, including length (L), width (W) and thickness (T).

The bending samples were loaded in 3-point bending until failure to determine the ultimate flexural strength and flexural modulus. The tensile samples were unable to be successfully completed due to the limitations of the current machinery available and the high elongation of the material. These coupons will be tested later, outside the scope of this work. The SEM samples were examined using both polished and non-polished samples.

Results and Discussion

The FLOW3D-Cast simulations were run for all nine combinations of sprues and plate thicknesses. In Figure 2.11, the defect areas for each simulation are shown. It can be seen that much of the defects are present in the center of the casting, especially for the 15mm plates. The helical samples show the least amount of defects present in the main casting cavity, with some defects in the runner and gate.

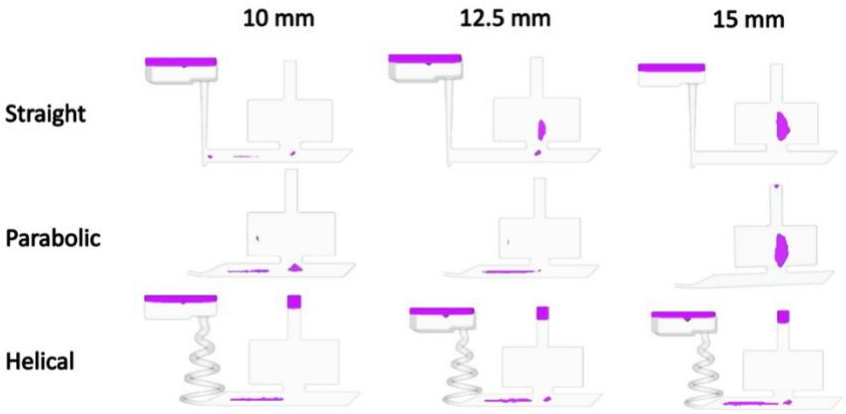

Figure 2.11. FLOW3D-Cast simulation results showing defect areas for each sprue (Straight, Parabolic, and Helical) and plate thickness (10mm, 12.5mm, and 15mm) combination.

Table 2.3. Maximum and average entrance velocity measurements for each combination of sprue type and plate thickness, including respective fill times.

Thickness	**Straight**			**Parabolic**			**Helical**		
	Max. Vel. (m/s)	Avg. above 0.5 m/s (m/s)	Fill Time (s)	Max. Vel. (m/s)	Avg. above 0.5 m/s (m/s)	Fill Time (s)	Max. Vel. (m/s)	Avg. above 0.5 m/s (m/s)	Fill Time (s)
10 mm	1.54	1.19	2.42	1.14	0.88	3.72	0.44	0	4.4
12.5 mm	1.51	1.15	2.86	1.09	0.88	4.06	0.44	0	4.78
15 mm	1.63	1.17	3.2	1.1	0.88	4.62	0.42	0	5.0

Table 2.4. Two-factor ANOVA without replication for gate velocity above 0.5 m/s.

Source of Variation	**SS**	**df**	**MS**	**F**	**P-value**
Sprue	2.22740	2	1.11370	8352.75	0.000
Thickness	0.00027	2	0.00013	1.00	0.444
Error	0.00053	4	0.00013		
Total	2.22820	8			

Table 2.5. Two-factor ANOVA without replication for maximum gate velocity.

Source of Variation	**SS**	**df**	**MS**	**F**	**P-value**
Sprue	1.92976	2	0.964878	527.90	0.000
Thickness	0.00216	2	0.001078	0.59	0.596
Error	0.00731	4	0.001828		
Total	1.93922	8			

From the results in Table 2.3, the straight sprue had both the highest maximum and average entrance velocity measurements for all combinations. This was expected based on results previous works and reaffirms the hypotheses. In addition, the fill time of the straight sprues is the shortest, which makes sense given the metal has the shortest distance to travel and it is traveling at the highest velocity out of all three types when it enters the main cavity. The fill time for the helical sprue was nearly double that of the straight sprue, while the inlet velocity was roughly one quarter that of the straight sprue. In most cases, this additional time will likely be negligible. The results of the ANOVA study on gate entrance velocity greater than 0.5 m/s and maximum entrance velocity are shown in Tables 2.4 and 2.5 respectively. From Table 2.4, the ANOVA results determined that the sprue geometry had a significant effect on the velocities above 0.5 m/s. However, the plate thickness was shown to not be statistically significant on the velocities above 0.5 m/s. The ANOVA results for maximum gate velocity in Table 2.5 determined that the plate thickness did not have a significant effect on maximum gate velocity. However, the sprue geometry was shown to be statistically significant for the gate velocities.

It was hypothesized the straight sprue would have the highest percent defect, as the geometry causes a significant amount of turbulence and mixing of the oxide film layer that is created during filling. Both the parabolic and helical sprues attempt to reduce this effect by slowing the molten metal during pouring and creating a smooth channel with no abrupt angles that would increase mixing. The parabolic sprue did reduce the velocity and defects compared the straight sprue, but the helical sprue was the best on average.

Table 2.6. Percent defect (%) for each plate from CT analysis with the respective sprue type.

Plate	**Percent Defect (%)**
Straight 1	0.419
Straight 2	0.540
Straight 3	0.485
Straight 4	0.814
Straight 5	0.357
Average	**0.523**
Parabolic 1	0.494
Parabolic 2	0.537
Parabolic 3	0.293
Parabolic 4	2.34
Parabolic 5	1.12
Average	**0.957**
Helical 1	0.222
Helical 2	0.300
Helical 3	0.505
Helical 4	0.637
Helical 5	0.637
Average	**0.460**

Table 2.7. Two-factor ANOVA without replication for defect percentage.

Source of Variation	Adjusted SS	df	Adjusted MS	F	P-value
Type	0.05059	2	0.02530	0.43	0.663
Error	0.65108	11	0.05919		
Total	0.70167	13			

Table 2.6 shows the results of the percentage defect calculation from the CT analysis. The Parabolic sprue had the highest average percent defect, while the Helical sprue had the lowest. With a resolution of 124 micrometers, some defects may have not been fully captured by the CT results. In Figure 2.12, much of the defects are positioned in the center of the plates. The cause of these defects can be the result of turbulence during casting; however, other factors may have played a role. While CT data only shows a change in density, the location of the defects in Figure 2.13 shows a side view of samples from each sprue type, locating the defects closer to the center of the cavity than the walls. This means that most defects are likely filling defects as opposed to shrinkage during cooling.

Additionally, the vents for the plates were not sized properly, resulting in a shrinkage cavity near the top center of the plates. Due to this, when calculating the percent defect, this area was removed from the calculation to better compare the effects of the sprue geometries. Table 2.7 contains the results of the two-factor ANOVA test. Parabolic 4 and Straight 4 had values that were more than double that of the next highest in their group. And such, Parabolic 4 and Straight 5 were removed from ANOVA study due being statistical outliers. From this ANOVA study, it can be seen that the sprue geometry was not statistically significant on the percent defect.

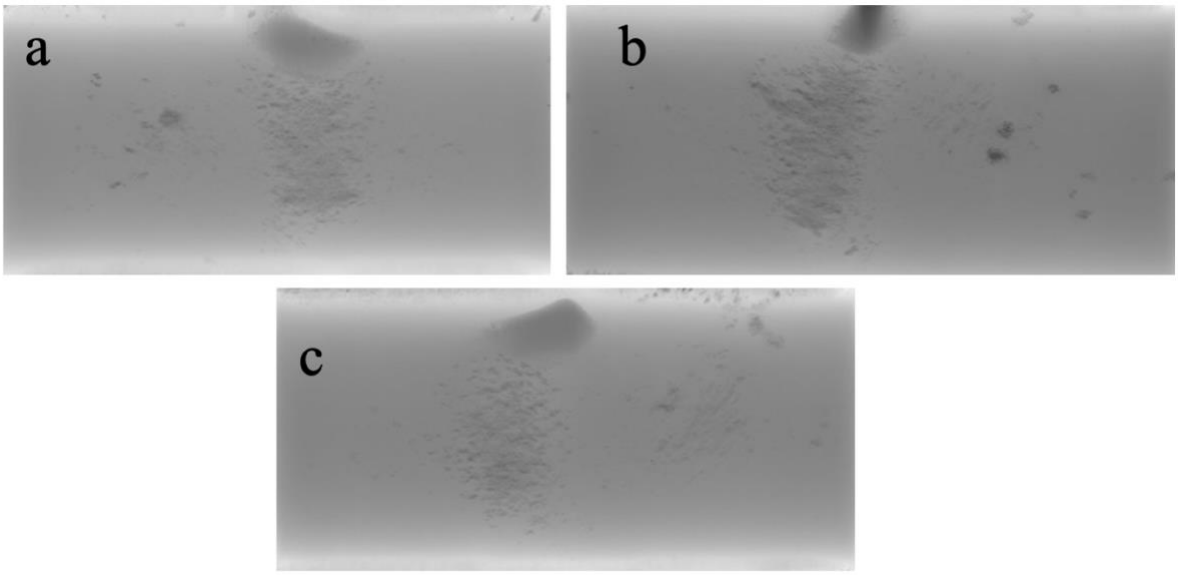

Figure 2.12. CT data showing front views of straight (a), parabolic (b) and helical (c) samples.

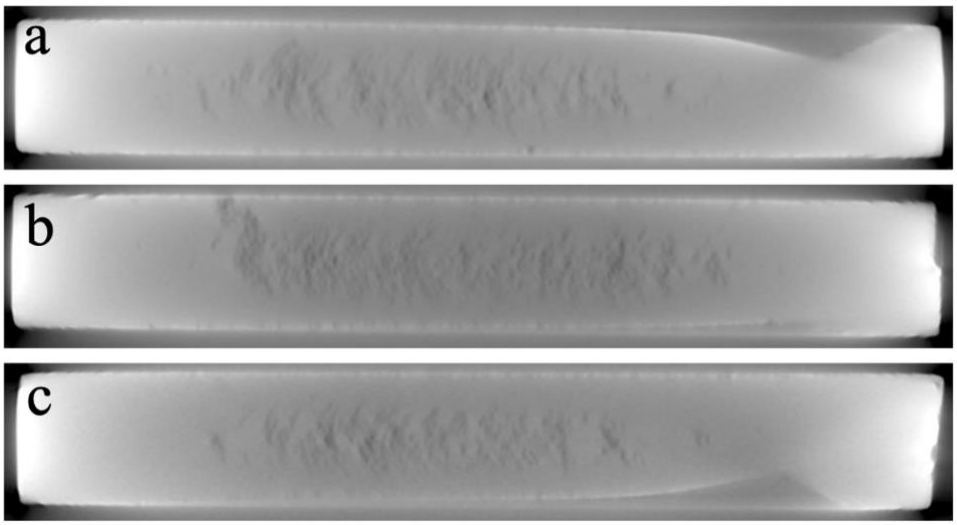

Figure 2.13. CT data showing side views of straight (a), parabolic (b) and helical (c) samples.

The bending experiments used the ASTM E290-14 samples cut earlier. All 12 samples were bent following ASTM standards and the ultimate flexural strength (UFS) and flexural modulus were recorded. Figure 2.14 shows the boxplot for UFS. While the means for each sprue type were not determined to be statically significant, the change in standard deviation should be noted. The standard deviation for the helical samples was less than 10% of that of the straight sprue samples. For certain critical applications, there may be value reducing the standard deviation. And such, it is recommended that this be explored in further research. Also, while testing, the bearings slightly shifted and while the flexural modulus was unaffected, the UFS results could have errors and additional testing would be helpful.

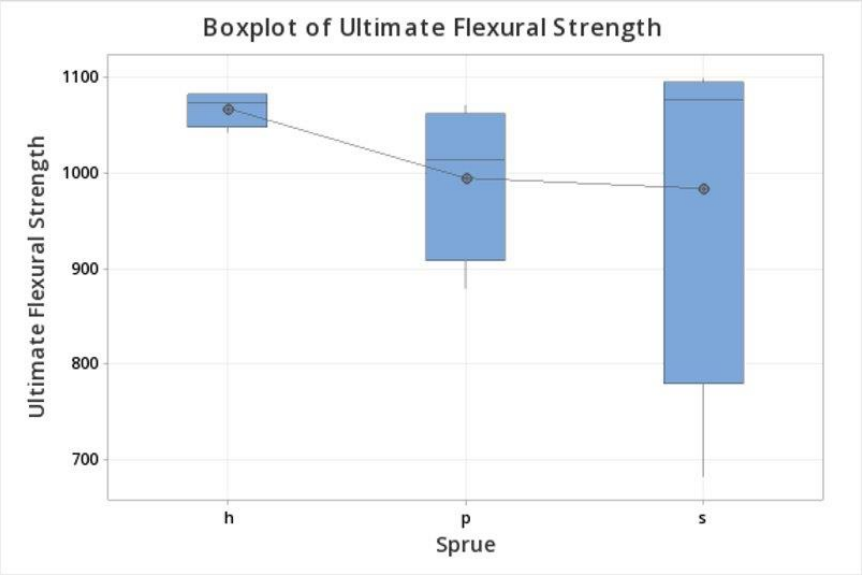

Figure 2.14. Boxplot of ultimate flexural strength as a function of sprue type helical (h), parabolic (p) and straight (s).

The flexural modulus had more conclusive results, showing an over 7% increase in helical sprue compared to straight sprue (Figure 2.15). The Fisher test at 95% confidence was able to show statistical difference of means between the straight and helical samples (Figure 2.16). Since the ultimate flexural strength is sensitive to a change in microstructure and the microstructure of all samples was similar, it is expected that the UFS would be similar across all samples. However, the flexural modulus is more sensitive to defects and porosity, so given the helical plates had the lowest defects, an increase in flexural modulus is also expected.

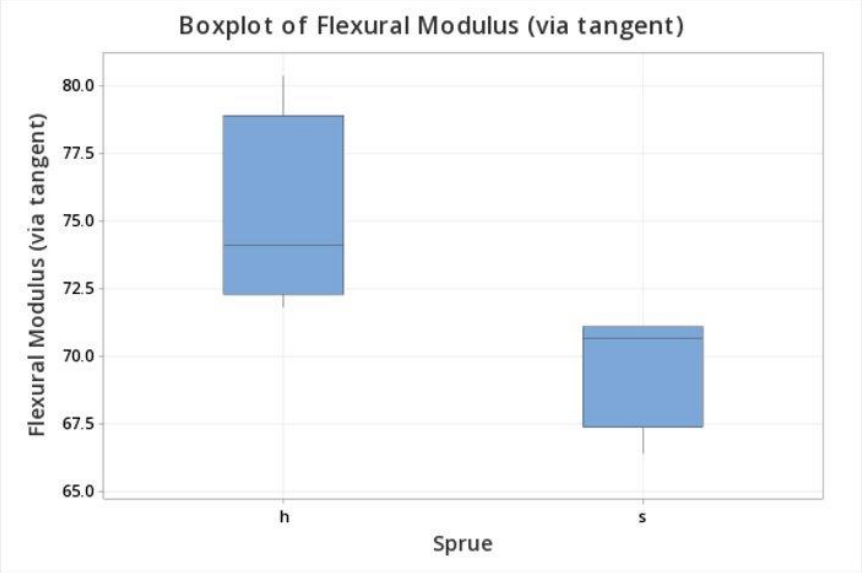

Figure 2.15. Boxplot of flexural modulus as a function of sprue type, helical (h) and straight (s).

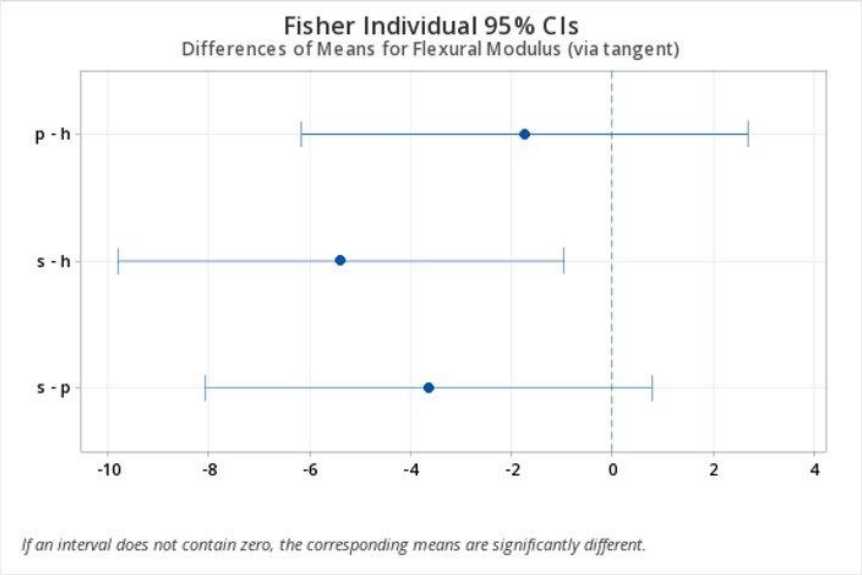

Figure 2.16. Fisher test of flexural modulus as a function of sprue type, helical (h) and straight (s).

SEM imagery results were obtained from the 10 x 10 mm samples from the 12 plates for both polished and unpolished samples. Figure 2.17 shows images of a polished helical sample at various zoom levels and both 20 kV and 10 kV power levels. Distinct microstructure can be observed in Figure 2.15c with long columnar grains and smaller, dark globular structures.

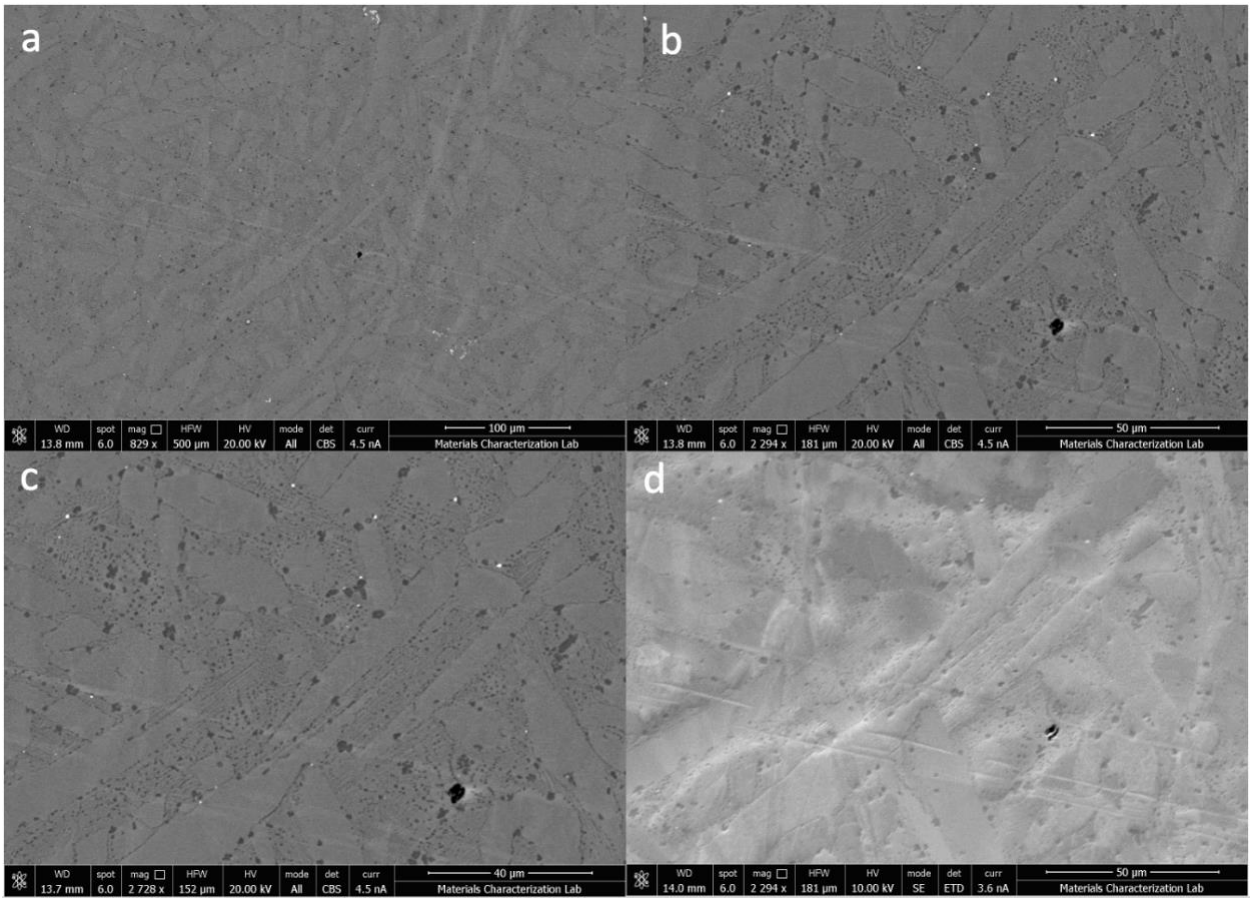

Figure 2.17. SEM images for Helical sprue samples; a-c are at different magnification levels with the CBS detector and d uses the ETD detector.

In Figure 2.16, SEM images of each sprue type are shown, with the similar magnification levels. Figure 2.18a is from a Helical sprue sample, Figure 2.18b is from a Parabolic sprue sample, and Figure 2.18c is from a Straight sprue sample. It should be noted that Figure 2.18c is at 10kV power level and uses the CBS detector, while Figure 2.18a and b are at 20 kV using the ETD detector. Comparing images from the three sprue types in Figure 2.18, no immediate differences can be seen. Microstructure between each image is somewhat similar with both long columnar grains as we as the small, dark globular grain structures. Much of this can be attributed to the similar pouring conditions between all samples, the cooling curve is known to have a direct impact on the grain growth. Future work on these samples is recommended, involving heat treatment to modify grain structures for more ideal properties.

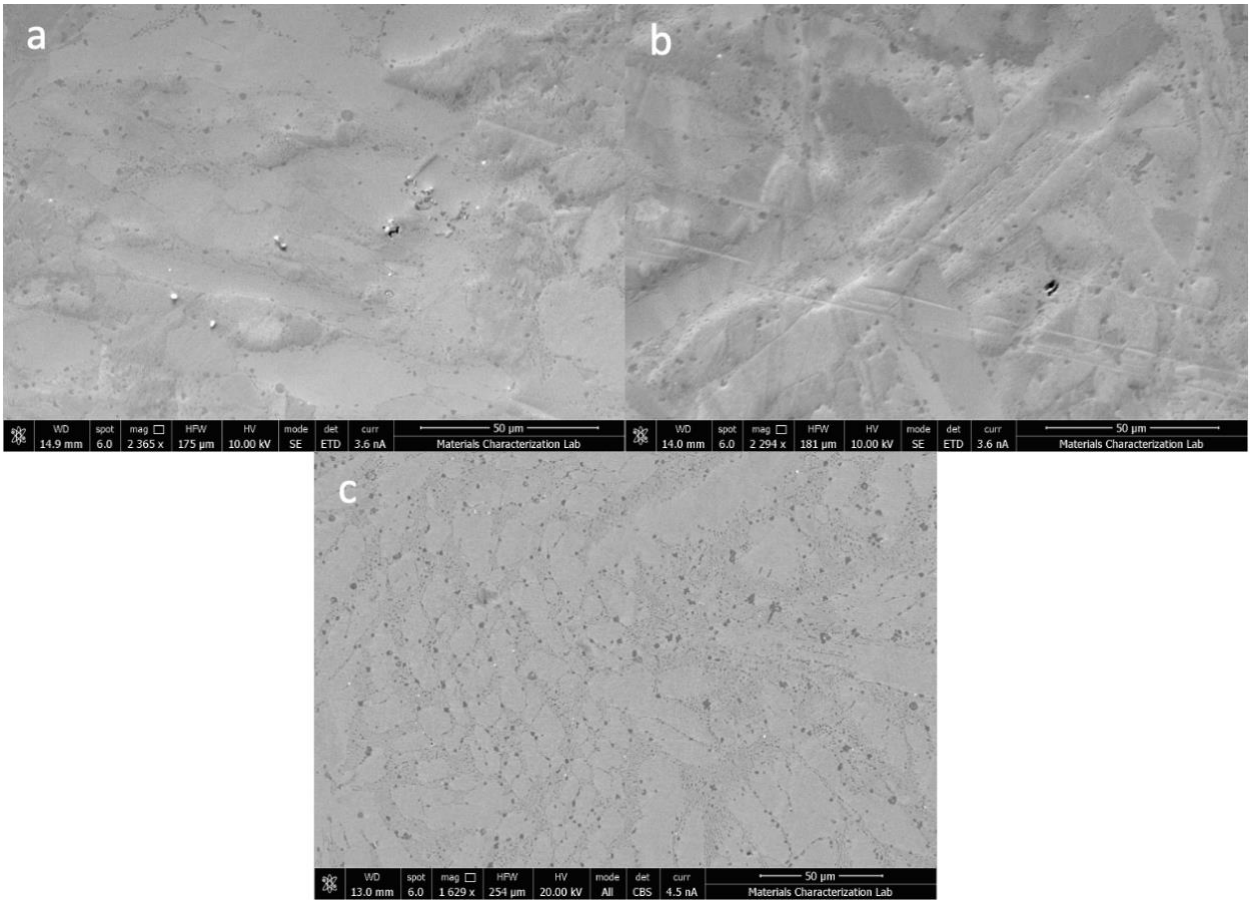

Figure 2.18. SEM images for Helical (a) Parabolic (b) and Straight (c) sprue samples. Note Straight sprue (c) uses CBS detector, while (a) and (b) used ETD.

Conclusions

Nickel-Aluminum Bronze has very desirable qualities such as high strength and corrosion resistance, making it ideal for naval and marine applications. While most NAB castings are traditionally sand-cast, this work has shown how using more complex sprue geometries can lower in-gate velocity and defects in castings. This study was focused on incorporating 3D printing technology into the sand-casting process to allow for these complex geometries to be cast. Straight, Parabolic, and Helical sprues were used and their effects on the entrance velocity, defect percentage, flexural modulus, and microstructure were studied. It was found that both the maximum entrance velocity and average velocity above 0.5 m/s were the lowest for the helical sprue. The defect percentage from CT analysis also determined the helical sprue samples to have the least number of defects on average. The bending analysis resulted in the helical sprue exhibiting over 7% higher flexural modulus than the straight sprue. The SEM images exhibited similar grain structures among all samples tested. Future work on tensile testing and heat treatment of SEM samples is recommended.

CONCLUSION

Metal casting has proven to be a mainstay in modern life, with most people interacting with cast objects on a daily basis. The science of metal casting is an ancient process and the basic processes have mostly remained unchanged. New technologies such as 3D-printing and advanced CFD solvers have allowed for advancement in metal casting. When combined with a process such as sand casting, sand molds are able to be 3D printed with complex sprue geometries such as helical and parabolic shapes. These geometries have been shown to reduce the entrance velocity of the metal during casting which can lead to reduced defect and entrained air. Nickel-Aluminum Bronze is a common alloy used for marine and naval applications and was the focus of this study. The goal was the investigate the effects that novel sprue geometries had on casting quality, mechanical properties, and microstructure of the NAB castings. It was found that the helical sprue produced the lowest maximum entrance velocity, and did not allow the velocity to exceed 0.5 m/s. The helical sprue also had the lowest defect percentage on average, while maintaining a flexural modulus 7% higher than that of the straight sprue. Since all samples produced similar SEM imagery, it is recommended that future work be conducted on heat treating the SEM samples.

REFERENCES

1. Curle, U. A., Wilkins, J. D. & Govender, G. Industrial semi-solid rheocasting of aluminum A356 brake calipers. *Adv. Mater. Sci. Eng.* **2011**, (2011).
2. Grosselle, F., Timelli, G., Bonollo, F., Tiziani, A. & Della Corte, E. Correlation between microstructure and mechanical properties of Al-Si cast alloys. *Metall. Ital.* **101**, 25–32 (2009).
3. Karunakar, D. B. & Datta, G. L. Prevention of defects in castings using back propagation neural networks. *Int. J. Adv. Manuf. Technol.* **39**, 1111–1124 (2008).
4. Taricco, G. (CM T. & Mascetti, S. (XC E. Investigation of Mould Leakages in a Gravity Casting. Available at: https://www.flow3d.com/investigation-of-mould-leakages-in-a-gravity-casting/. (Accessed: 7th July 2020)
5. Gondkar, V. S. & Inamdar, K. H. Optimization of Casting Process Parameters through Simulation. *Int. J. Appl. or Innov. Eng. Manag.* **3**, 276–283 (2014).
6. Reis, A., Xu, Z., Tol, R. V. & Neto, R. Modelling feeding flow related shrinkage defects in aluminum castings. *J. Manuf. Process.* **14**, 1–7 (2012).
7. Oh-Ishi, K. & McNelley, T. R. Microstructural modification of as-cast NiAl bronze by friction stir processing. *Metall. Mater. Trans. A Phys. Metall. Mater. Sci.* **35 A**, 2951–2961 (2004).
8. Hunt, L. B. The long history of lost wax casting - Over five thousand years of art and craftsmanship. *Gold Bull.* **13**, 63–79 (1980).
9. Khan, M. A. A., Sheikh, A. K. & Al-Shaer, B. S. *Evolution of metal casting technologies—a historical perspective*. *SpringerBriefs in Applied Sciences and Technology* (2017). doi:10.1007/978-3-319-46633-0_1
10. Grand View Research. *Metal Casting Market Size, Share & Trends Analysis Report By Material (Aluminum, Iron, Steel), By Application (Automotive & Transportation, Building & Construction, Industrial), By Region, And Segment Forecasts, 2019 – 2025*. (2019).
11. Sama, S. R., Badamo, T., Lynch, P. & Manogharan, G. Novel sprue designs in metal casting via 3D sand-printing. *Addit. Manuf.* **25**, 563–578 (2019).
12. Kang, J. *et al.* Additive manufacturing-driven mold design for castings. *Addit. Manuf.* **22**, 472–478 (2018).
13. Kang, J. wu & Ma, Q. xian. The role and impact of 3D printing technologies in casting. *China Foundry* **14**, 157–168 (2017).
14. Wang, J., Sama, S. R. & Manogharan, G. Re-Thinking Design Methodology for Castings: 3D Sand-Printing and Topology Optimization. *Int. J. Met.* **13**, 2–17 (2019).
15. Hodder, K. J. & Chalaturnyk, R. J. Bridging additive manufacturing and sand casting: Utilizing foundry sand. *Addit. Manuf.* **28**, 649–660 (2019).
16. Culpan, E. A. & Rose, G. Microstructural characterization of cast nickel aluminium bronze. *J. Mater. Sci.* **13**, 1647–1657 (1978).
17. Culpan, E. A. & Rose, G. Corrosion behaviour of cast nickel aluminium bronze in sea water. *Br. Corros. J.* **14**, 160–166 (1979).
18. Lorimer, G. W., Hasan, F., Iqbal, J. & Ridley, N. Observation of microstructure and corrosion behaviour of some aluminium bronzes. *Br. Corros. J.* **21**, 248–244 (1986).
19. Aviva Metals. Nickel Aluminum Bronze Alloys. Available at: https://www.avivametals.com/collections/nickel-aluminum-bronze. (Accessed: 28th December 2020)

20. Anantapong, J., Uthaisangsuk, V., Suranuntchai, S. & Manonukul, A. Effect of hot working on microstructure evolution of as-cast Nickel Aluminum Bronze alloy. *Mater. Des.* **60**, 233–243 (2014).
21. Ai, Y. *et al.* Effect of heat treatment on microstructure and properties of NCu30-4-2-1 alloy. *Jinshu Rechuli/Heat Treat. Met.* **40**, 107–110 (2015).
22. Hanke, S., Fischer, A., Beyer, M. & dos Santos, J. Cavitation erosion of NiAl-bronze layers generated by friction surfacing. *Wear* **273**, 32–37 (2011).
23. Nimbulkar, S. L. & Dalu, R. S. Design optimization of gating and feeding system through simulation technique for sand casting of wear plate. *Perspect. Sci.* **8**, 39–42 (2016).
24. Huang, P. H. & Lin, C. J. Computer-aided modeling and experimental verification of optimal gating system design for investment casting of precision rotor. *Int. J. Adv. Manuf. Technol.* **79**, 997–1006 (2015).
25. Wang, D. *et al.* Rapid casting of complex impeller based on 3D printing wax pattern and simulation optimization. *Int. J. Adv. Manuf. Technol.* **100**, 2629–2635 (2019).
26. Tavakoli, R. & Davami, P. Optimal riser design in sand casting process with evolutionary topology optimization. *Struct. Multidiscip. Optim.* **38**, 205–214 (2009).
27. Shangguan, H., Kang, J., Deng, C., Hu, Y. & Huang, T. 3D-printed shell-truss sand mold for aluminum castings. *J. Mater. Process. Technol.* **250**, 247–253 (2017).
28. American Foundry Society. About Metal Casting. Available at: https://www.afsinc.org/about-metalcasting. (Accessed: 25th October 2019)
29. American Foundry Society. Industry Statistics. Available at: https://www.afsinc.org/industry-statistics. (Accessed: 25th October 2019)
30. Tyler, D., Aluminum, G., Co, M., Pischel, R. & Metallurgical, F. Permanent Mold Casting. *Casting* **1**, 689–699 (2018).
31. Sama, S. R., Wang, J. & Manogharan, G. Non-conventional mold design for metal casting using 3D sand-printing. *J. Manuf. Process.* **34**, 765–775 (2018).
32. Upadhyay, M., Sivarupan, T. & El Mansori, M. 3D printing for rapid sand casting—A review. *J. Manuf. Process.* **29**, 211–220 (2017).
33. Chhabra, M. & Singh, R. Rapid casting solutions: A review. *Rapid Prototyp. J.* **17**, 328–350 (2011).
34. Ciobanu, I., Munteanu, S., Crisan, A., Bedo, T. & Monescu, V. Riser analysis using casting simulation techniques during solidification. *Int. J. Met.* **8**, 63–75 (2014).
35. Bernard, A., Delplace, J. C., Perry, N. & Gabriel, S. Integration of CAD and rapid manufacturing for sand casting optimisation. *Rapid Prototyp. J.* **9**, 327–333 (2003).
36. Cheah, C. M., Chua, C. K., Lee, C. W., Feng, C. & Totong, K. Rapid prototyping and tooling techniques: A review of applications for rapid investment casting. *Int. J. Adv. Manuf. Technol.* **25**, 308–320 (2005).
37. Pattnaik, S., Karunakar, D. B. & Jha, P. K. Developments in investment casting process - A review. *J. Mater. Process. Technol.* **212**, 2332–2348 (2012).
38. Wang, J., Sama, S. R., Lynch, P. C. & Manogharan, G. Design and Topology Optimization of 3D-Printed Wax Patterns for Rapid Investment Casting. *Procedia Manuf.* **34**, 683–694 (2019).
39. Liu, Q., Sui, G. & Leu, M. C. Experimental study on the ice pattern fabrication for the investment casting by rapid freeze prototyping (RFP). *Comput. Ind.* **48**, 181–197 (2002).
40. Taşcioğlu, S. & Akar, N. A novel alternative to the additives in investment casting pattern wax compositions. *Mater. Des.* **24**, 693–698 (2003).

41. Guharaja, S., Noorul Haq, A. & Karuppannan, K. M. Optimization of green sand casting process parameters by using Taguchi's method. *Int. J. Adv. Manuf. Technol.* **30**, 1040–1048 (2006).
42. Ghomashchi, M. R. & Vikhrov, A. Squeeze casting: An overview. *J. Mater. Process. Technol.* **101**, 1–9 (2000).
43. Lakeshore Die Cast. Die Casting Cost. Available at: http://www.lakeshorediecast.com/die-casting-cost.html.
44. Konopka, Z., Zyska, A., Łą, M. & Nadolski, M. The influence of the composite casting wall thickness on the arrangement of particulate within the matrix. *Arch. Foundry Eng.* **8**, 89–92 (2008).
45. Die Casting Limits Size. Available at: http://ppcpinc.com/die-casting-limits-size/. (Accessed: 7th July 2020)
46. Campbell, J. *Complete Casting Handbook: Metal Casting Processes, Metallurgy, Techniques and Design: Second Edition*. (Butterworth-Heinemann, 2015). doi:10.1016/C2014-0-01548-1
47. Hsu, F. Y., Jolly, M. R. & Campbell, J. A multiple-gate runner system for gravity casting. *J. Mater. Process. Technol.* **209**, 5736–5750 (2009).
48. Bhatt, H., Barot, R., Bhatt, K., Beravala, H. & Shah, J. Design Optimization of Feeding System and Solidification Simulation for Cast Iron. *Procedia Technol.* **14**, 357–364 (2014).
49. Song, J. *et al.* A review on hot tearing of magnesium alloys. *J. Magnes. Alloy.* **4**, 151–172 (2016).
50. Akhyar, H., Malau, V., Suyitno & Iswanto, P. T. Hot tearing susceptibility of aluminum alloys using CRCM-Horizontal mold. *Results Phys.* **7**, 1030–1039 (2017).
51. Zhao, D., Guo, W., Zhang, B. & Gao, F. 3D sand mould printing: a review and a new approach. *Rapid Prototyp. J.* **24**, 285–300 (2018).
52. Frazier, W. E. Metal additive manufacturing: A review. *J. Mater. Eng. Perform.* **23**, 1917–1928 (2014).
53. Dutta, B. & Sam Froes, F. H. The additive manufacturing (AM) of titanium alloys. *Titan. Powder Metall. Sci. Technol. Appl.* **1019**, 447–468 (2015).
54. Henderson, H. B. *et al.* Additively Manufactured Single-Use Molds and Reusable Patterns for Large Automotive and Hydroelectric Components. *Int. J. Met.* **14**, 356–364 (2019).
55. Almaghariz, E. S. *et al.* Quantifying the role of part design complexity in using 3d sand printing for molds and cores. *Int. J. Met.* **10**, 240–252 (2016).
56. Shivpuri, R., Cheng, X., Agarwal, K. & Babu, S. Evaluation of 3D printing for dies in low volume forging of 7075 aluminum helicopter parts. *Rapid Prototyp. J.* **11**, 272–277 (2005).
57. Armillotta, A., Baraggi, R. & Fasoli, S. SLM tooling for die casting with conformal cooling channels. *Int. J. Adv. Manuf. Technol.* **71**, 573–583 (2014).
58. ExOne | Sand 3D Printers – Sand Printing & Casting.
59. Norican Group. DISA General Specifications.
60. Mohiuddin, M. V., Hussainy, S. F., Krishnaiah, A. & Laxminarayana, P. Experimental investigation to produce thin-walled sand casting using combination of casting simulation and additive manufacturing techniques. *Int. J. Adv. Manuf. Technol.* **90**, 3147–3157 (2017).
61. Al-Hashem, A. & Riad, W. The role of microstructure of nickel-aluminium-bronze alloy

on its cavitation corrosion behavior in natural seawater. *Mater. Charact.* **48**, 37–41 (2002).
62. Wu, Z., Cheng, Y. F., Liu, L., Lv, W. & Hu, W. Effect of heat treatment on microstructure evolution and erosion-corrosion behavior of a nickel-aluminum bronze alloy in chloride solution. *Corros. Sci.* **98**, 260–270 (2015).
63. Hazra, M. & Balan, K. P. Failure of a nickel aluminium bronze (NAB) canned motor pump impeller working under polluted sea water – Influence of material selection, section thickness dependent microstructure and temper annealing heat treatment. *Eng. Fail. Anal.* **70**, 141–156 (2016).
64. Lv, Y., Wang, L., Han, Y., Xu, X. & Lu, W. Investigation of microstructure and mechanical properties of hot worked NiAl bronze alloy with different deformation degree. *Mater. Sci. Eng. A* **643**, 17–24 (2015).
65. Ni, D. R., Xue, P. & Ma, Z. Y. Effect of multiple-pass friction stir processing overlapping on microstructure and mechanical properties of as-cast NiAl bronze. *Metall. Mater. Trans. A Phys. Metall. Mater. Sci.* **42**, 2125–2135 (2011).
66. Ni, D. R., Xiao, B. L., Ma, Z. Y., Qiao, Y. X. & Zheng, Y. G. Corrosion properties of friction-stir processed cast NiAl bronze. *Corros. Sci.* **52**, 1610–1617 (2010).
67. King, P., Martinez, D. & Manogharan, G. Novel Sprue Designs to Reduce Casting Defects in Nickel-Aluminum Bronze: A Computational Study. in *Proceedings of the ASME 2020 15th International Manufacturing Science and Engineering Conference* (2020).
68. Bradski, G. The OpenCV Library. *Dr. Dobb's J. Softw. Tools* (2000).
69. Thermo Fisher Scientific. Avizo. (2022).